Characterization and modeling of high-value inductors in ELF band using a Vector Network Analyzer

Rosa M. García, José A. Gázquez, *Member, IEEE,* and Nuria Novas

Abstract- Characterization and modeling of high-value inductors (hundreds to thousands of henrys) is a complex problem, exacerbated when working in the Extremely Low Frequency (ELF) range. This paper details the measurement and characterization of inductors using a Vector Network Analyzer that has a bottom operating frequency of 5 Hz. Using this device, we establish a strategy for measuring the impedance of high-inductance coils - with or without a high-permeability core - and propose an mathematical model that can explain the behavior of these high-inductance coils, which incorporate long lengths of winding wire, as a function of working frequency. These inductors were constructed as part of a research project on ELF electromagnetic fields. The importance of making a complete characterization derives from the need to exploit the largest possible amount of energy captured by the coil, which acts as a sensor. As part of the characterization process, we propose a mixed model of concentrated and distributed parameters that fits the experimental results with an error of about 2 % for the frequency range 5 to 500 Hz. The effects of the magnetic core have been characterized in terms of concentration of the magnetic field, its effect on inductance and winding resistance, as a function of frequency.

***Index Terms* --Inductor model, ELF measurement, vector network analyzer, transmission lines, cores.**

I. INTRODUCTION

THE measurement of high-value inductors in the low and very low frequency range is a complex issue. There are several factors affecting the classic model of inductors and, in order to achieve a correct characterization, we need tools that can determine the real and imaginary impedance of the system as a function of frequency. Since the appearance of the first coils in spring 1891 by Nikola Tesla [1], there has been a need to characterize and model the behavior of these elements, as they become increasingly applied in science and industry. The elements characterized include non-linear frequency effects, which lead to equations that are not linearly proportional to the frequency. Examples include the effect on impedance of the element due to parasitic capacitance between turns of the coil, and ohmic resistance of the winding.

Various methods for measuring inductors have evolved over time, from very basic ones to ones based on the latest technological developments. The classic methods were first used in the early 20th century, and were based on the application of Ohm's law and calculation of the time constant of the evolution of the current when the coil was connected to a battery.

The discovery of the oscilloscope in 1897 by Ferdinand Braun [2], allowed the phase shift, voltage, and current of the coils to be studied. Despite the antiquity of these methods, they appear in recent studies, albeit with various modifications. An example is the study cited in [3]; which demonstrates how effective the use of a voltmeter and current meter is for measuring inductance in the order of nanohenries. This and other studies show the simplicity and validity of these methods when the degree of precision required is not high.

Subsequently, an instrument was developed that revolutionized the field of measurement: the LCR meter. This induction meter uses discrete measurement frequencies to measure voltage by periodically interrupting the current and using a fixed operating frequency. The use of LCR meters has boomed in the last decade, as demonstrated by the number of published papers featuring them. Different papers compare LCR meters available on the market today [4], methods of calibration for these instruments [5], and determine their performance and uncertainty under standard conditions [6]. These tools allow a relatively simple process of measurement, with an acceptable degree of uncertainty, greatest when the frequency range is in the order of kHz. However, none of these methods determines high impedance with great precision; nor do they offer the possibility of choosing the frequency range for measurement, premises required for achieving greater accuracy in the characterization of these elements. As a result, new techniques have appeared in recent years that have revolutionized classic methods, which are based on reflection factors of pulse signals [7] or signal dispersion [8]. New devices have also been developed, such as the vector network analyzer (VNA), a special type of which is used in this study. The VNA allows determination of both the real and imaginary impedance values of an element in the frequency range established, the frequency range being the distinguishing feature. Measurement of inductance using these tools is a hot topic, as shown by the large number of papers on the subject. In source [9] we see a very recent study on the use of a VNA for measurement in the VHF band (Very High Frequency), between 30 MHz and 300 MHz. Until now, most studies using VNAs devised to measure characteristics of inductors have focused on higher frequencies, with the operating frequency typically being in the order of kHz. One of the difficulties encountered when working at low frequencies is the need for high acquisition times, given that by decreasing the frequency, the time necessary for establishing values with the required precision increases, and multiple cycles are required to identify the mode and phase of a magnitude. If the frequency is very low, the measurement time cycle is longer, T=1/f. However, the present study is carried out in the low frequency range, despite the length of time needed to take measurements. This is the feature that differentiates the study from others, because few instruments are available that can operate in this way.

Another feature that distinguishes the present study is the value of inductances and the frequency range considered, since most published studies have focused on measuring low-value inductors in the high-frequency band [10]. The measurement of very large coils is complicated by the multiple effects that manifest during the process, including the capacitance between turns, and phenomena arising from the winding behavior, such as transmission lines. In this article, we take both concepts into account, establishing a method for measuring high-value inductors in the ELF band of 5 to 500 Hz, based on the use of a very low frequency VNA to which is applied a particular configuration that takes into account the correct coupling between system elements so as to minimize any loss. The method is applied to characterizing coils designed for use as ELF magnetic sensors, which are capable of capturing the low amplitude of natural magnetic fields, such as Schumann resonances [11]. Schumann resonances are very weak signals, pT, generated in the earth-ionosphere cavity, which have a fundamental component at around 7 Hz. The study of these signals is of interest in diagnosing a variety of environmental features. One of the main difficulties of measuring this phenomenon lies in the design of the sensor. In addition to the measurement of these inductors, this paper presents a model that explains their behavior with frequency. To date, many theoretical models have been devised to explain the behavior of

certain standard inductors, such as RF (radio frequency) chokes and tuning inductors, depending on their operating frequency range [12]. Most of these theoretical methods are based on the lumped parameters, ignoring the distributed parameters that may be related to the effect of transmission lines in the coil. In our study, the effects related to transmission lines that we propose appear as a consequence of the very long winding compared to the wavelength of the signals applied. The proposed model is a hybrid model, which considers the effect of lumped and distributed parameters, and its dependence on frequency in the low frequency range.

II. COILS FOR MEASURING ELF FIELDS

Signals for measuring the Schumann resonance are located in the frequency range 7 Hz to 100 Hz, with vacuum wavelengths of 43000 km to 3000 km, respectively. An electric dipole antenna would have huge dimensions and so it is more appropriate to use a magnetic antenna. The development of a coil with a large number of windings is not an innovation, although it is of interest due to its size, the wire used, its configuration and the large number of technical difficulties solved during the process (such as wire breakage during the winding process if it is too thin). In this paper, we highlight how an element with these characteristics can be applied as an ELF sensor. Until now, magnetometers and magnetic antennas used for similar purposes have had very different characteristics: most have small dimensions and small-diameter wire (less than 0.1 mm), which implies a high internal resistance, primary resonance at low frequencies, and a small S/N ratio. The behavior of an inductor is governed by the Faraday-Lenz law (1), [13].

$$V_e = -\frac{d\Phi}{dt} \tag{1}$$

The area of the coil winding is constant, but the magnetic field is not stationary, and so the induced voltage in the system for signals with sinusoidal components is given by (2):

$$V_e = -nA\frac{\partial B}{\partial t} \tag{2}$$

The work of these coils is to capture external magnetic fields; this depends quadratically on the radius of the turns and linearly on their number. Therefore, the optimum configuration, given an equal winding weight, is a single turn of maximum area, so confirming the need for large turns on the coil winding.

For sinusoidal signals, in the presence of thermal noise, the S/N ratio for the coil output is given by (3). We observe that, for a given field B and measuring frequency of ω_k, the ratio increases with $1/\sqrt{R}$, where R is the real part of the coil impedance at the frequency of the selected component, ω_k, K is the Boltzmann constant, T the temperature in degrees Kelvin, W is the bandwidth of the amplifier system, n the number or turns and A the average area of the coil.

$$S/N(\omega_k) = \frac{\overline{B}\,\omega_k nA}{\sqrt{4KTWR}} \tag{3}$$

There are two alternatives for improving the efficiency of the coil: increase the number of turns, n, and the resistance, or establish coils with low-resistance winding. In our prototype we decided to develop a coil with many turns of considerable size, with the least resistance possible within the available budget and a maximum S/N ratio (3), as shown in Fig. 1. The number of turns could have been greater and each turn of a smaller size, but this would have increased

the resistance of the system, giving rise to a less favourable S/N ratio and a higher internal impedance, so making the extraction of energy from the coil more difficult.

The dimensions of the coil are shown in Table I, where l_{coil} is the height of the coil, l_t is the total winding length, d is the diameter of the coil, d_{coil} the interior diameter, n the total number of turns and d_{turns} their average diameter. The characteristics of this coil are different from other traditional inductors [14], and it is therefore of interest to determine how it behaves at different frequencies.

Fig. 1. ELF magnetic sensor prototype.

TABLE I

DIMENSIONAL PARAMETERS FOR PROTOTYPE SENSOR

Dimensions					
l_{coil} (cm)	D (cm)	d_{coil} (cm)	l_t (km)	N	d_{turns} (cm)
80	34	7	27.8	58450	16

TABLE II

MAGNETIC PROPERTIES OF FERROMAGNETIC MATERIAL

Properties	Value
Initial Permeability	60000
Maximum Permeability	300000
Saturation induction	0.63 T
Remanence	0.39 T
Coercivity	0.80 A/m
Resistivity 20ºC	60 μΩ-cm
Curie Temperature	400 ºC

To increase the field captured by a coil, we can introduce a core of high-permeability magnetic material. The presence of the core modifies the characteristics of the inductor [15], and provides a multiplier effect of the capture area, due to the properties of these materials in external magnetic fields. Although the inclusion of a core increases the internal impedance of the sensor, the signal received is larger and the S/N ratio is increased. The choice of material for the high-permeability ferromagnetic core was complicated, requiring a thorough study of the magnetic properties and

applications of commercially-available ferromagnetic materials [16]. The material chosen was a soft alloy of nickel, iron, copper and molybdenum [17]. Table II shows some of its properties; of which its high magnetic induction and permeability are of particular note. The core is made from stacked sheets of material, which allows it to operate better at low frequencies [18], from 10 Hz to several kHz. In addition, using this process reduces potential losses due to Foucault currents [19], as the measurement process (see below) demonstrates.

III. TECHNIQUE FOR MEASURING IMPEDANCE

This section discusses the methodology for measurement and how it is applied in to determine impedance as a function of frequency for both the high-value coreless coil and the coil enclosing various ferromagnetic cores.

A. Measurement technique: the vector network analyzer

Of the existing methods for measuring impedance, the method based on determining the reflection factor of a signal for each frequency interval is currently the most accurate for determining both the real and imaginary impedance as a function of frequency in networks with one or two ports. The basic method used by vector network analyzers (VNA) excites a test network with bursts of different frequencies for each interval, then the corresponding reflection factor is measured in phase and quadrature. Reducing the frequency increases the time interval required for measurement, and so the development of equipment capable of taking measurements at low frequencies is the main constraint.

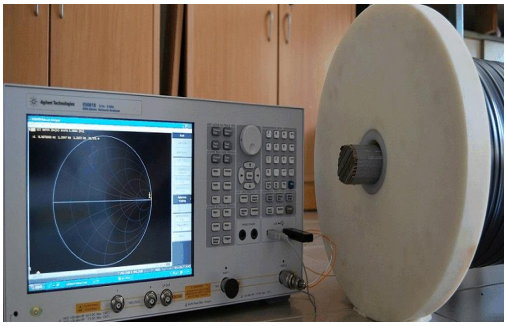

Fig. 2. Vector Network Analyzer, E5061B.

In this study, we used the Agilent VNA E5061B [20], a special device that has recently appeared on the market (Fig. 2). It is capable of taking measurements from 5 Hz upwards. The method used in this study for measuring impedance uses one port and the representation in the format used by Smith [21]. The configuration of the instrument must also consider the type of calibration, since the type of calibration and standards used can have a significant impact on the accuracy of the measurements obtained [22]. In low-frequency analyzers, the most commonly-used calibration method is SOL (short-open-load), whereby we calibrate the system in short circuit, in open circuit and with a reference load. Nonetheless, high-frequency systems also offer other methods of calibration, such as thru-reflect-line (TRL), line-reflect-match (LRM), and line-reflect-reflect-match (LRRM). In addition, advanced techniques that move calibration standards on-chip can increase accuracy. Another aspect that must be considered is the effect of imperfect load standards and mismatched impedance values, which lead to significant loss of accuracy, of between 0.2% to 0.5% of the actual measurement. Through this measurement technique we achieve a good coupling between system elements and the minimization of losses in the system. The accuracy of the process was checked by comparison with a reference impedance of 50 Ω.

B. Impedance measurements

This section describes the behavior of the real and imaginary impedance of a inductor with either an air-core or a ferromagnetic one at different frequencies using a particular configuration in our VNA. To determine the effect of different cores, we developed 4 cores of the ferromagnetic material chosen above, of various length and diameter (between 4 and 4.55 cm). The arguments employed in choosing these cores concerned the optimization of the free area in the interior of coil. Table III shows the characteristics of each of the cores tested, further indicating whether waxed paper was placed between the layers (only cores 2 and 4). Due to the extreme sensitivity of the instrument used, we performed a large number of measurements; all measurements are reproducible.

TABLE III

FERROMAGNETIC CORES TESTED

Core	Diameter (cm)	Length (m)	Waxed paper
Core 1	4.00	1	-
Core 2	4.52	1	X
Core 3	4.46	2	-
Core 4	4.52	2	X

Fig. 3 shows the representation of the real part of the impedance of the air-coil, and of the coil containing each of four ferromagnetic cores, over frequencies from 5 to 500 Hz.

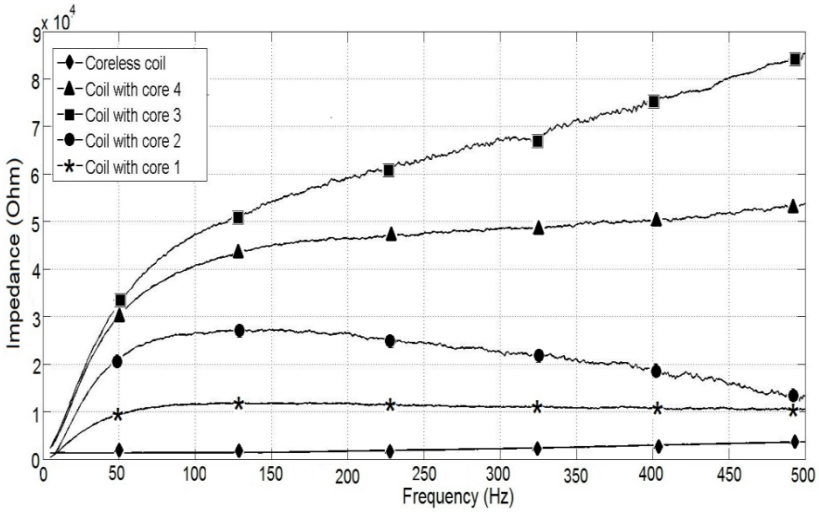

Fig. 3. Representation of the real part of the system impedance.

Fig. 4 shows the imaginary part of the impedance of the air-coil and of the same coil with different test cores inserted. As in the previous case, the air-coil gives the lowest impedance values, increasing with the length of the core used. From this graph, we can determine the coefficient of self-inductance that appears in each situation, and confirm the effect of the presence of a core inside the coil. The imaginary impedance curve can be fitted in the frequency range close to the origin (5Hz), where we observe a linear trend. VNA can measure the real and imaginary impedance of the system separately, and so the resistance value does not affect the measurement of the imaginary part (which is the part used for fitting).

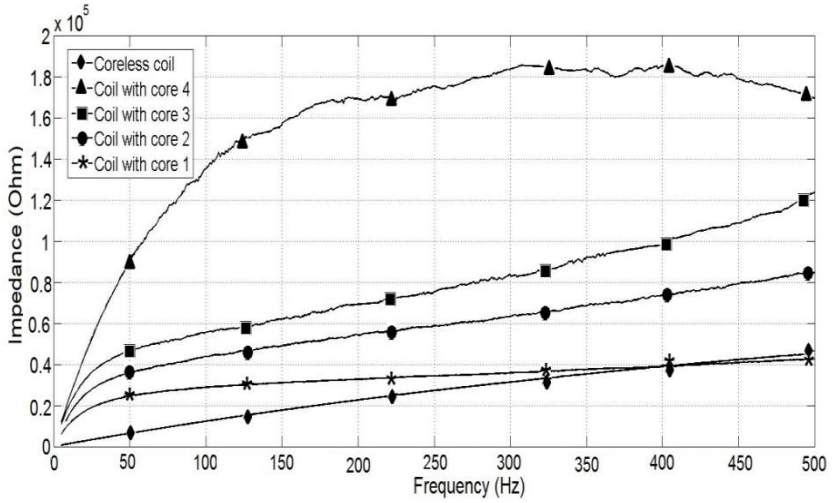

Fig. 4. Representation of the imaginary part of the system impedance.

In order that the system acts as the ELF sensor we determined its behavior in the ELF range, from 7 – 100 Hz; however, measurements may be extended to 500 Hz and this may be of interest to others. From Fig. 3, we can compare the impedance for the air-coil and the coil containing the ferromagnetic cores, for frequencies of 5 to 500 Hz. The curve of the air coil represents the lowest impedance, which relates to the resistance of the coil due to the winding. The value of the real part of the impedance increases with frequency due to the effects of selective adaptation of the capacity between turns, along with other distributed effects that will be described later.

Determining the behavior of the coil as different types of cores are introduced is quite complex; the highest value of the real part of the impedance is obtained with core 3, the largest core, with no electrical insulation, and this effect is related to Foucault current losses. The presence of an electrical insulator between the plates that comprise core 4 produces a smaller increase in the real part of impedance with frequency. Both cores 3 and 4 show the same increasing trend up to frequencies of 50 Hz. When we shorten the length of the core by half, core 2, we reach a point of maximum impedance in the curve. We observe that the cores with smaller diameter and shorter length yield lower impedance values.

Achieving a good fit at the low frequency end of the curve is desirable, since this is the area least affected by the non-quantifiable effects that come from using the magnetic materials that comprise the core. Table IV shows the coefficients of self-inductance achieved with each of the configurations. As expected, the value obtained with the air-coil is by far the smallest, confirming that a ferromagnetic core greatly increases the self-inductance of the system. By introducing a core, the inductance increases by an order of magnitude compared to the inductance value for the air-coil. Like the graph in Fig. 4, the table reflects how inductance increases in longer cores. Core length is a fundamental parameter in the design; the core must be as long as possible to obtain the best results. In addition, we tested the influence of two factors that reduce the loss due to Foucault currents, namely lamination of the core and the presence of special waxed paper between layers. Both actions help to decrease the value of the real part of the impedance and so increase the energy transferred by the sensor to the measurement system; as shown by the impedance curves of the core 4, the core selected to build the definitive ELF sensor.

TABLE IV

SELF-INDUCTANCE OBTAINED

TEST SITUATION	Inductance (H)
ir-coil	21.61
Coil with core 1	135.09
Coil with core 2	182.87
Coil with core 3	244.73
Coil with core 4	398.98

The ELF sensor has a balanced winding, consisting of two parallel wire windings; each of which is represented by the high induction air-coil considered in this study. Both windings have identical characteristics and so only one of them was used to carry out the process of measurement and modeling. Since the total number of coil turns is greater, so the expected inductance value in the sensor will be approximately 4 times that expressed in Table IV for each of the configurations studied.

IV COIL MODELING

Due to the peculiarities of the develop system, the high number of turns, its size and the presence or not of a ferromagnetic core, the behavior of system with frequency needs to be known accurately.

A. Behavior of the air coil

We begin by analyzing the impedance presented by the air coil. The complex part of the impedance increases linearly with frequency; however, the most significant effect is seen in the real part, this factor also affects the thermal noise generated by the coil (3). In an ideal resistive element, the real part of the impedance is kept almost completely constant. In this coil, the real part of its impedance increases significantly with frequency, from close to 1300 Ω to values four times higher. To explain this, we developed a theoretical model to fit the behavior of the real part of the air-coil in the frequency range studied, *i.e.*, from 7 Hz to 500 Hz. The increase of the impedance with frequency in the coil has a complex trend and it cannot be fitted using any common mathematical function, as shown in Fig. 5. The classic model [23] established for standard coils does not fit the measurements obtained with this type of inductor for our range of operating frequencies; these frequencies correspond to wavelengths of around one hundredth of the length of the coil winding, beyond which diverse distributed phenomena begin to appear. A number of studies developed in recent years accord in that an inductor can be modeled with an equivalent circuit in RF (as in Fig. 6 (a), where R, L and C represent the equivalent resistance, inductance and distributed parasitic capacitance between turns. This is the classic model of distributed parameters and is not suitable for coils with short and medium lengths of wire. As discussed above, the behavior of the coil in the first frequency interval (closest to the origin) fits this lumped parameter model. This model is an inductor model for RF signals; nevertheless, it is a valid model over the range of frequencies used in our study, since the concept of low frequency diminishes at high values of L. In this system we can determine all parameters except the capacitance between turns. This is the only parameter that cannot be determined by direct measurement, but must be simulated using the block model. In our case, we obtained a capacitance between turns in the coil of 2074 nF, a value consistent with the results obtained by applying a theoretical method such as the finite element method (FEM) [24]. The real part of impedance at low frequencies is determined by equation (4), where X_c and X_L are the

capacitive and inductive reactance of the circuit. Depending on the frequency of the system and its features, their values can be calculated by equations (5) and (6). The fit of this impedance curve, taken to be the impedance curve of lumped parameters with real values, is good up to frequencies of around 150 Hz.

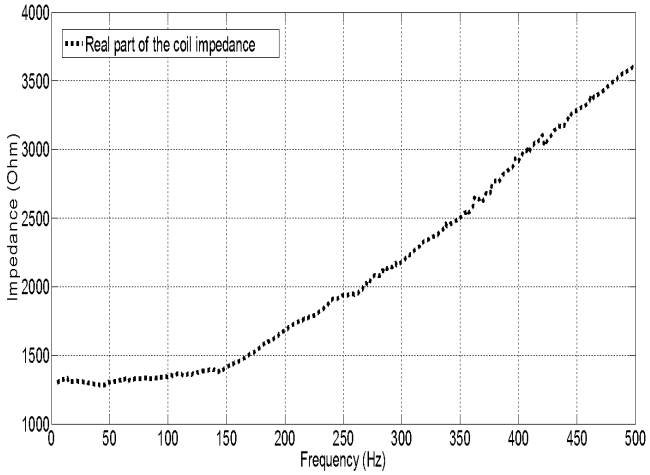

Fig. 5. Real part of the impedance of the coreless coil.

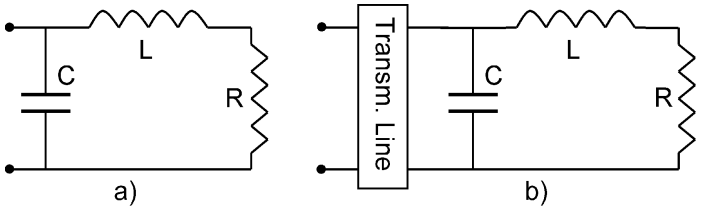

Fig. 6. Circuits of the model of behavior in the coreless inductor.

$$\mathrm{Re}(Z) = \frac{RX_c^2}{R^2 + \left(X_L - X_c\right)^2} \tag{4}$$

$$X_L = 2\Pi f L \tag{5}$$

$$X_c = \frac{1}{2\Pi f C} \tag{6}$$

The error was less than 1%, as shown in Fig. 7. In complex high-inductance inductors, such as the one developed for this study, there are a number of effects that are incompatible with the previous lumped parameter model. From 150 Hz, phenomena related to distributed parameters begin to appear in the coil; these are complex parameters that cannot be located in a particular region of space. The appearance of these distributed effects is due to the influence of the long length of coil thread compared to the signal wavelength tested. We found that, for lengths of wire of about 28 km, these effects are observed at frequencies around 100 Hz, corresponding to 0.01λ. The determination of these distributed parameters is highly complex. To date, several studies have attempted to model distributed-parameter systems using sophisticated mathematical tools [25]. An example is described in [26], which establishes a numerical method using second order spatial derivatives. These methods are too costly from a computational point of view, and do not give an easily reproducible physical significance. For this reason, in the present study, we have attempted to find a model that fits the actual data which, in turn, gives the system the simplicity needed for reproduction on other high-value inductors.

The experimental curve shows that an almost perfectly linear trend begins to appear at above 150 Hz. This linear portion can be explained theoretically using the Smith Chart representation of impedances [21]. We observe a linear

increase in impedance with frequency, so that the impedance of the system moves towards that of a generator. As the frequency increases, the effects due to the presence of transmission lines (in this case, the inductor winding) in the system become more marked. Transmission lines are complex elements, whose behavior varies according to their geometry, the materials used for conductors and the signal frequency. They exhibit a number of parameters that can be determined experimentally, such as the propagation speed and characteristic impedance.

Using expression (7), we can calculate the impedance of a transmission line [27], where Z_L and Z_0 are the load impedance and characteristic impedance of the transmission line, respectively, and λ is its wavelength.

$$Z_t(\lambda) = Z_0 \frac{Z_L \cos(2\Pi\lambda) + jZ_0 sin(2\Pi\lambda)}{Z_0 \cos(2\Pi\lambda) + jZ_L sin(2\Pi\lambda)} \tag{7}$$

However, for high frequencies, and in systems with large values of inductance, (200 Hz can be considered as high frequency), we do not consider that the impedance of the system is due solely to the impedance of the transmission lines. Therefore, the predominant effects in the first frequency band are combined with the effects of the transmission lines. We determined that, in the second frequency interval, the model that best fits the behavior of the coil consists of the effect of transmission lines in cascade with the block circuit associated with an inductor in the primary frequency band (Fig. 6 (b)). The real part of the impedance of this system is represented by equation (8), while equations (9), (10), (11) and (12) represent the terms corresponding to the real and imaginary impedance of the inductor block Z_b, and the impedance due to transmission lines Z_t.

$$\mathrm{Re}(Z) = \frac{Z_{t_R}{}^2 Z_{b_R} + Z_{t_R} Z_{b_R}{}^2 + Z_{t_R} Z_{b_I}{}^2 + Z_{t_I}{}^2 Z_{b_R}}{\left(Z_{t_R} + Z_{b_R}\right)^2 + \left(Z_{t_I} + Z_{b_I}\right)^2} \tag{8}$$

$$Z_{b_R} = \frac{RX_c{}^2}{R^2 + \left(X_L - X_c\right)^2} \tag{9}$$

$$Z_{b_I} = \frac{X_L X_c{}^2 - X_L{}^2 X_c - R^2 X_c}{R^2 + \left(X_L - X_c\right)^2} \tag{10}$$

$$Z_{t_R} = \frac{Z_0{}^2 Z_L}{Z_L{}^2 + \left(Z_0{}^2 - Z_L{}^2\right)\cos^2(2\Pi\lambda)} \tag{11}$$

$$Z_{t_I} = \frac{Z_0 \sin(4\Pi\lambda)\left(Z_0{}^2 - Z_L\right)}{2\left[Z_L{}^2 + \left(Z_0{}^2 - Z_L{}^2\right)\cos^2(2\Pi\lambda)\right]} \tag{12}$$

In Fig. 7, we see the alignment of the experimental curve with the model curve. Taking into account the distributed effects, there is an error of less than 2% at frequencies above 210 Hz. Using this model, we can theoretically determine the characteristic parameters of the transmission line, such as the propagation speed of 0.228c and characteristic impedance of 2.180 kΩ. Both values are close to those obtained experimentally, thus demonstrating the validity of the model. We can also calculate other electrical constants, such as the lumped parameters of the transmission line. These

parameters are the series inductance and the distributed capacity, of 31.8 μH and 6.7 pF, respectively. Both are consistent with typical values for conventional transmission lines.

The final model consists of two functions, one for the lower frequency band and one for the upper range, plus an intermediate frequency range for which there is no complete alignment to the experimental curve. This frequency range of this transition zone is very narrow compared with the overall range of study, extending from 150 to 210 Hz. In this zone, the maximum error is 10% and we must look for another function to decrease this error. The transition zone covers the transition from the model for a very-low-frequency inductor to the model where distributed effects predominate. The shift in frequencies is not instantaneous, and therefore, a transition zone is required to delineate the part of the curve where these effects become increasingly significant.

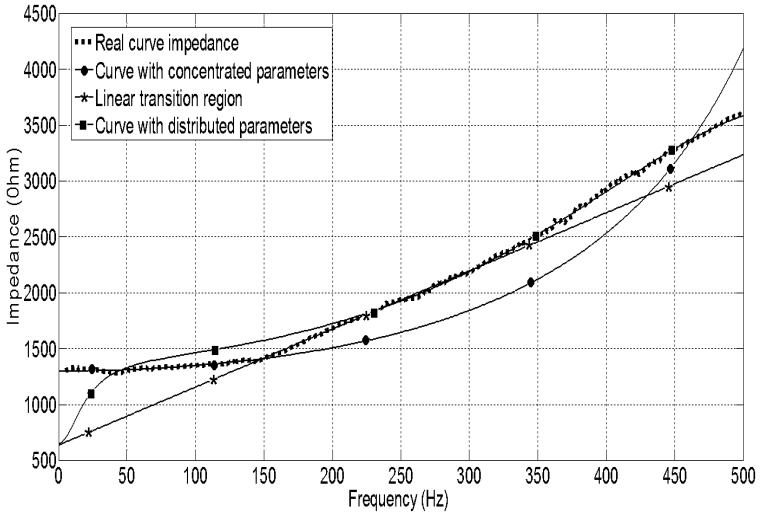

Fig.7. Curve of real impedance of the coil and each of the curves of the model.

$$\mathrm{Re}(Z)=\begin{cases}\dfrac{RX_c^{\,2}}{R^2+\left(X_L-X_c\right)^2} & 5\le f<150\\[2ex] \dfrac{3\left(Z_0+L\right)}{Z_L}f+R/2 & 150<f<210\\[2ex] \dfrac{Z_{t_R}^{\,2}Z_{b_R}+Z_{t_R}Z_{b_R}^{\,2}+Z_{t_R}Z_{b_I}^{\,2}+Z_{t_I}^{\,2}Z_{b_R}}{\left(Z_{t_R}+Z_{b_R}\right)^2+\left(Z_{t_I}+Z_{b_I}\right)^2} & 210\le f\le 500\end{cases} \tag{13}$$

The function applied to the transition zone is an empirical function, whose constants can be related to model parameters at low-frequency, and to the characteristic parameters of the system´s transmission lines.

Equation (13) shows the definitive model for describing the behavior of the real part of the impedance of the high induction air coil inductors, over the entire range of frequencies studied, from 5 to 500 Hz. It is a piecewise function, comprising a sequence of three frequency intervals, whose fit to the frequency data is shown in Fig. 7.

In Fig. 8, we clearly observe that the theoretical model, consisting of three frequency ranges, can be fitted to the data for the real impedance of the coil with a minimum error of 0.5%. We can therefore state that the model we have used is appropriate for predicting the behavior of our high-inductance coil in the frequency range studied. We must take into account that this is not an intuitive model, but it does possess a high degree of reproducibility. The model has been

tested for other high-inductance air-coils containing fewer turns, and gives an acceptable fit. There were differences in the frequency range of the transition zone, and in the frequency above which the effects of distributed parameters predominate. The empirical nature of the transition zone means that it would be difficult to establish a correlation technique. However this is a topic with many possible paths of development.

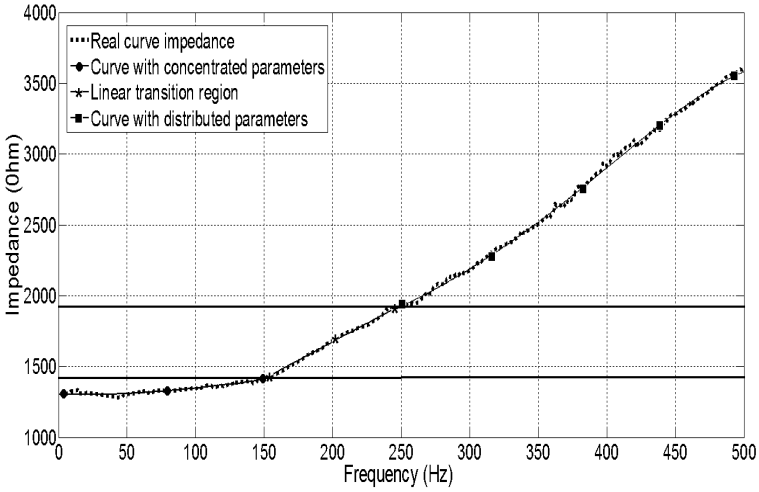

Fig. 8. Final alignment of the actual impedance curve and the theoretical model.

We expect normal inductors at very low frequencies to behave like an RLC circuit (considering very low frequencies to be those at the low end of the range included in this study). Nevertheless, we find that for somewhat higher frequencies (but still considered within the low frequency band), special high-inductance coils show behavior normally associated with high-frequency phenomena, such as the effects of the transmission lines.

B. Behavior of the coil with core

After taking the measurements described in Section II and due to complex, frequency-dependent effects associated with the core, namely Foucault current, hysteresis loss, permeability variation with frequency, etc., it was not possible to establish a model of the coil with core in the same way as for the air coil, described in the previous section. . Rather, studying the behavior of the coil with magnetic core is focused on determining the effects of the magnetic core on increasing the field detected by the coil.

To calculate the magnetic field existing inside a core, we consider its geometry; the problem is equivalent to the resolution of magnetic field inside a magnetized cylinder with radius, r_{core} and length l_{core} [28].

In a widely-varying magnetic field, the majority of materials have a linear behavior, like ferromagnetic materials, where the magnetization vector is proportional to the applied field. According to the theory of magnetization of currents, [29] we define the magnetizing currents by volume and surface area. If we consider magnetization in the material to be constant, the magnetized cylindrical core behaves as a cylindrical sheet through which a surface current circulates, and the field sources are bands of thickness dz. The problem is similar to the calculation of the magnetic field of a circular loop of radius r_{core} and current I at a point on the z axis, (14):

$$\overline{B}(z) = \frac{\mu_0 I \ {r_{core}}^2}{2\left(z^2 + {r_{core}}^2\right)^{3/2}} \quad \overline{u_z} \tag{14}$$

Similarly, the field created along the z-axis by each of the bands making up the cylindrical core of our problem and carrying a magnetization moment M, can be integrating it over the entire length of the core, l_{core} , to obtain the magnetic field at any point along the z-axis (15).

$$\overline{B}_{in}(z)=\frac{\mu_0\ M}{2}\left[\frac{\frac{z}{l_{core}}}{\sqrt{\left(\frac{z}{l_{core}}\right)^2+\left(\frac{r_{core}}{l_{core}}\right)^2}}-\frac{\frac{z}{l_{core}}-1}{\sqrt{\left(\frac{z}{l_{core}}-1\right)^2+\left(\frac{r_{core}}{l_{core}}\right)^2}}\right]\ \overline{u_z} \tag{15}$$

The magnetization of the material can be considered as a linear function for small values of the magnetic field (16), where H_i is the intrinsic field of the material; it depends on the applied field H_a and the demagnetizing field H_d.

$$M=\chi_m H_i=\chi_m\left(H_a+H_d\right)=\chi_m\left(H_a-NM\right) \tag{16}$$

The demagnetizing field is fitted to the applied field by means of a correction factor called the demagnetizing factor, N [30]. This factor is only calculated accurately for ellipsoids. Cylindrical samples have two types of demagnetizing factors: the magnetometric demagnetizing factor, N_m, and the fluxmetric demagnetizing factor, N_f. According to [31] the most appropriate factor for cylindrical coils is Nm, which relates to the magnetization in the whole sample and not to the magnetization of the equatorial plane (Nf), although in this case, the difference between the two values, according to the tables presented in many studies [32], is very small.This factor depends on the susceptibility of the system, χ, and the relationship between the length and the diameter of the sample.

Equation (17) expresses the magnetizing of the sample as a function of the applied field, the demagnetizing factor, N_f, and the permeability magnetic, μ, given that $\chi_m=\frac{\mu-\mu_0}{\mu_0}=\mu_r-1$

$$M=\left(\frac{\mu-\mu_0}{\mu_0+N_m\mu-N_m\mu_0}\right)H_a \tag{17}$$

Substituting (17) into (15), we obtain the magnetic flux density present in the interior of a cylindrical sample as a function of the applied field and the other system parameters (18).

$$B_{in}(z)=\left(\frac{\mu_0(\mu-\mu_0)}{2\left[\mu_0+N_m(\mu-\mu_0)\right]}\right)\left[\frac{\left(\frac{z}{l_{core}}\right)}{\sqrt{\left(\frac{z}{l_{core}}\right)^2+\left(\frac{r_{core}}{l_{core}}\right)^2}}-\frac{\left(\frac{z}{l_{core}}-1\right)}{\sqrt{\left(\frac{z}{l_{core}}-1\right)^2+\left(\frac{r_{core}}{l_{core}}\right)^2}}\right]H_a \tag{18}$$

Assuming that the external magnetic field at any point away from the core is constant, $B_{out}=\mu_o H_a$, the ratio of the magnetic fluxes over an arbitrary surface, due to the field outside and inside the core, is expressed by equation (19). Fig. 9 graphically represents the flux ratio for the selected core 4 for various values of permeability, since it is an unknown magnitude. The permeability of the system is less than that provided by the manufacturer of the material (table II) because this magnitude depends on the working conditions under which it is determined (low frequencies and fields).

$$\frac{\Phi_{in}}{\Phi_{out}}(z)=\left(\frac{(\mu_r-1)}{2[1+N_m(\mu_r-1)]}\right)\left[\frac{\left(\frac{z}{l_{core}}\right)}{\sqrt{\left(\frac{z}{l_{core}}\right)^2+\left(\frac{r_{core}}{l_{core}}\right)^2}}-\frac{\left(\frac{z}{l_{core}}-1\right)}{\sqrt{\left(\frac{z}{l_{core}}-1\right)^2+\left(\frac{r_{core}}{l_{core}}\right)^2}}\right] \tag{19}$$

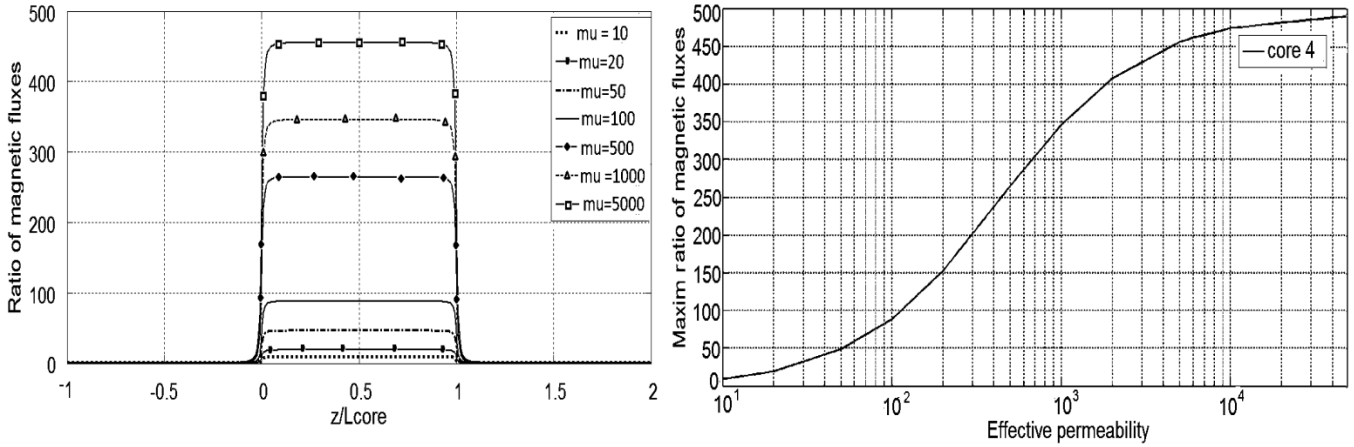

Fig. 9. Ratio of magnetic fluxes.

To determine the ratio of magnetic fluxes experimentally, we employ a transmitting coil of 2000 turns, connected to an signal generator with an output of up to 30 V, in the frequency range between 7 Hz and 50 Hz and located colinearly W=10 meters from the ELF sensor (Fig. 10) and we measure the voltage induced in the sensor coil with the core 4 and with the air coil. Experimentally, we obtain a ratio of magnetic fluxes that depends on frequency, that ranges between 20 and 100 for the most favored frequency, and thus the simulation (Fig. 9) is within this range.

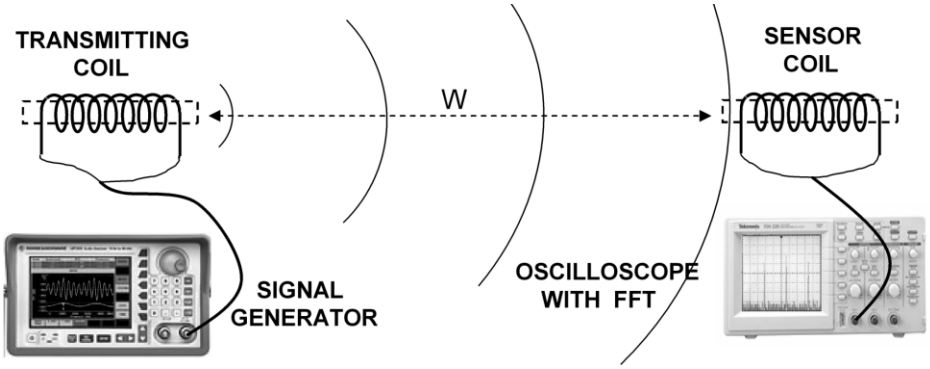

Fig. 10. Experimental gain core procedure.

CONCLUSIONS

The characterization of special coils, such as those used as ELF sensors, is key to the development of the measurement system. The measurement system depends on the energy delivered by the sensor, which becomes critical when the signal is too weak to be measured, as in the case of Schumann resonances. We have developed a model for high-inductance coils and long winding lengths that can be used as ELF sensors. Our new model includes the effects of transmission lines, which become evident at winding lengths exceeding 0.01λ of the signal. Using a vector network analyzer we are able to measure real and complex impedance as a function of frequency. We have characterized the system, so enabling a circuit to be designed that optimizes the energy captured by the sensor. From these data we are

able to determine the values of model parameters for an air-coil. We also studied the influence of using different ferromagnetic cores on the field strength inside and outside the coil. We propose a physical model that satisfactorily fits the experimental curve and explains the behavior of impedance versus frequency. Using this model we are able to make an initial determination of the effect of the lumped and distributed parameters that appear in the test air coil. The model is validated by the reproducibility of multiple measurements (greater than 5 in all situations) with the VNA.

ACKNOWLEDGMENTS

This work was forms part of Project FQM-32080 funded by the Ministry of Innovation, Science and Enterprise (Andalusian Regional Government). It was also funded from the European Union FEDER program, as part of Research Group TIC-019 "Electronics, Communications and Telemedicine", University of Almeria.

REFERENCES

[1] J. C. Mackechnie, "Nikola Tesla and the induction motor," *Electronics and Power*, vol. 15, no. 12, Dec. 1969, pp. 436-440.

[2] W. Margulis and S. Lava, "Oscilloscope measurement of picoseconds voltage," *Applied Physics Letters*, vol. 40, no. 9, May. 1982, pp. 829-831.

[3] C. Hsia, M. Lai and W. Feng," On-board effective inductance measurement," *in Proc. APCCAS '02 Conf. Circuits and Systems Theory*, Asia-Pacif, 2002, pp. 443–446.

[4] B. Waltrip, S. Avramov-Zamurovic and A. Koffman, "Inductance measurement using a LCR meter and a current transformer interface*," in Proc. IMTC 2005 Conf. Instrumentation and Measurement Technology*, Ottawa, Canada, 2005, pp. 1005–1007.

[5] K. Suzuki, "A new self-calibration method of an LCR meter for RF resistance calibration using capacitance standards," *IEEE Trans. Instrum. Meas.*, vol. 58, no. 4, Apr. 2009, pp. 993-996.

[6] A. Pokatilow, A. Satrapinski, T. Kübarsepp, "Verification of performance of commercial LCR meters," *in Proc. Conf. on Precision Electromagnetic Measurements*, Daejeon, Korea, 2010, pp. 408-409.

[7] M. V. Rojas-Moreno, G. Robles and B. Tellini, "Study of an inductive sensor for measuring high frequency current pulses," *IEEE Trans. Instrum. Meas.*, vol. 60, no. 5, May. 2001, pp. 1893-1900.

[8] M. Rojas, G. Robles and B. Tellini, "An inductive transducer for the measurement of high frequency pulses with applicability in the detection of partial discharge*," in Proc. IEEE IMTC*, 2010, pp. 375-379.

[9] W. B. Kuhn, A. P. Boutz, "Measuring and reporting high quality factors of inductors using vector network analyzers," *IEEE Trans. Microwave. Theory Tech.*, vol. 58, no. 4. Apr. 2010, pp. 1046-1055.

[10] A. Mamonov, "History and modern state of measurements of low inductance*," in: Proc. 7th Inter. Conf on Actual Problems of Electronic Instrument Engineering*, 2004, pp. 233.

[11] A. Yoshiaky and H. Hayakawa, "Recent studies of the Schumann resonance*," IEEJ Transactions on Fundamentals and Materials*, vol. 126, no. 1, 2006, pp. 28-30.

[12] Q. Yu and T. W. Holmes, "A study on stray capacitance modeling of inductors by using the finite element method," *IEEE Trans. Electromagn. Compat.*, vol. 43, no. 1, Feb. 2001, pp. 88–93.

[13] W. E. Gettys, F. J. Keller and M. J. Skove, *Physics Classical and Modern* (Book style). *McGraw-Hill*, 1991.

[14] G. Friesinger, S. Forster and U. Jeske, "Specific fabrication techniques of the polo model coil and its components," *IEEE Trans. Magn.*, vol. 28, Jan. 1992, pp.271-274.

[15] B. Hu, V. Tarateraseth and K. Y. See, "Assessment of electromagnetic interference suppression performance of ferrite core loaded power cord," *IET Sci., Meas. Technol.*, vol. 4, no. 4, Dec. 2010, pp. 229-236.

[16] H. I. Chan, K. W. E. Cheng and T. K. Cheung, "Study on magnetic materials used in power transformer and inductor," *in Proc. 2nd Inter. Conf. on Power Electronics Systems and Applications*, Dallas, TX, Jun. 165-169, 2006.

[17] The NILO and NILOMAG Nickel-Iron Alloys, Special Metals Products. [Online]. Available: http://www.specialmetals.com.

[18] G. Grandi, M. K. Kazimierczuk and A. Massarini, "Model of laminated iron-core inductors for high frequencies," *IEEE Trans. Magn.*, vol. 40, no. 4, Jul. 2004, pp. 1839-1845.

[19] I. Sebestyén, S. Gyimóthy and J. Pávó, "Calculation of losses in laminated ferromagnetic materials," *IEEE Trans. Magn.*, vol. 40, no. 2, March. 2004, pp. 924-927.
[20] Advanced measurements and modeling of differential devices manual, *Agillent Technologies*, (2006, Jun 1) [Online]. Available: http://www.home.agilent.com.
[21] C. Zelley, "A spherical representation of the Smith Chart," *IEEE Microwave Magazine*, vol. 8, no.3, Jun. 2007, pp. 60-66.
[22] "On-Wafer Vector Network Analyzer Calibration and Measurements," Cascade Microtech, Inc., Beawerton, OR, Application Note, 2002.
[23] H. Fujita, L. S. Petropoulos and M. A. Morich, "A hybrid inverse approach applied to the design of lumped-element RF coils," *IEEE Transaction on Biomedical Engineering*, vol. 46, no. 3, Mar. 1999, pp. 353-361.
[24] A. Massarini and M. K. Kazimierczuk, "Self-capacitance of inductors," *IEEE Transaction. Power Electronics*, vol. 12, no. 4, 1997, pp. 671-676.
[25] T. Colosi, E. H. Dulf and L. Buzdugan, "Modeling and numerical simulation method for systems with distributed parameters," *in Proc. 5th Inter. Symposium on Applied computational Intelligence and Informatics*, Timisoara, Romania, May. 2009.
[26] M. Sun, J. Moore and C. Zheng, "Soft constraints in identification on distributed parameters," *in Proc. 33rd Inter.Symposium on System Theory*, Southeastern, pp. 281-286, March, 2001.
[27] W. Warzanskyj, *Analysis of circuits* (Book style). E.T.S. Telecommunications Engineers, 1979, pp. 123–135.
[28] L. Landau and F. Lifchitz, *Electrodynamique des milieu continus, Physique théorique* (Book style). Mir, 1990
[29] B. García, *Fundamentals of electromagnetism* (Book style). University of Granada, 2005.
[30] J. A. Osborn, "Demagnetizing factors of the general ellipsoid," *Phys. Rev.*, vol. 67, 1945, pp. 351-357.
[31] R. I. Joseph, "Ballistic demagnetizing factor in uniformly magnetized cylinders," *J. Appl. Phys. Rev.*, vol. 37, 1966, pp. 4639-4643.
[32] D. X. Chen, J. A. Brug, R. B. Goldfarb, "Demagnetizing Factors for cylinders," *IEEE Trans. Magn.*, vol. 27, no. 4, Jul. 1999, pp. 3601-3619.

Rosa M García Salvador received her Physics degree from the University of Granada. Since 2008, she has been research and teaching assistant in the Computer Architecture and Electronics Department at the University of Almeria. Her research includes measurement systems and electromagnetic phenomena (email: rgs768@ual.es)

José A. Gázquez Parra (M'03) received his Ph.D. degrees in Telecommunications Engineering from the University of Malaga. He has been Associate Professor in the Computer Architecture and Electronics Department at the University of Almería since 1992. He was on the board of the company Engineering and Remote Control S.A. (Granada- Spain; 1991-1994). He is principal researcher of the Electronic Communications and Telemedicine (TIC019) Research Group of the Andalusian Research Plan. His research interests include measurement systems, telecontrol and embedded systems in real time. (email: jgazquez@ual.es)

Nuria Novas Castellano received her Ph.D. degrees in Electronic Engineering from the University of Almeria. She has been Associate Professor in the Computer Architecture and Electronics Department at the University of Almeria since 1999 and her research includes control systems and measurement. (e-mail: nnovas@ual.es)